# Analysis of microwave heating of copper powder compacts

K.I. Rybakov [a,*], M.M. Mahmoud [b,c,1], G. Link [d]

[a] Institute of Applied Physics, Russian Academy of Sciences, Nizhny Novgorod, 603950, Russia
[b] Mechanical Engineering Department, College of Engineering and Physics, King Fahd University of Petroleum and Minerals, Dhahran, 31261, Saudi Arabia
[c] Interdisciplinary Research Center for Advanced Materials, King Fahd University of Petroleum & Minerals, Dhahran, 31261, Saudi Arabia
[d] Karlsruhe Institute of Technology, IHM, Kaiserstr. 12, 76131, Karlsruhe, Germany

## HIGHLIGHTS

- Microwave heating of copper powder with oxide film on the particles has been analyzed.
- The indicative thickness of the oxide film has been determined from resistivity data.
- The complex permittivity and permeability of the copper powder have been calculated.
- The efficiency of microwave absorption in the copper powder has been assessed.
- The microwave energy needed for the oxide decomposition reaction has been determined.

## ARTICLE INFO

*Keywords:*
Microwave sintering
Metal powders
Thin copper oxide films
Modeling
Effective dielectric and magnetic properties

## ABSTRACT

The influence of the native oxide films, which is essential for the understanding of the microwave heating of metal powder, is analyzed numerically based on the experimental data on temperature, dilatation and resistance of compacted copper powder samples. The indicative thickness of the oxide films, determined from the resistivity data using an effective medium approximation, is shown to decrease from $\geq$1 μm to below 1 nm. The effective complex dielectric permittivity and magnetic permeability of the copper powder with oxide films on the particles are calculated within the recently developed models. The dielectric permittivity exhibits a percolation behavior in the temperature range of the oxide decomposition, viz. 210–250 °C when microwave heating is carried out in nitrogen and 330–375 °C – in argon. The efficiency of absorption of the incident 30 GHz microwave radiation in a slab of powder is assessed separately for the electric and magnetic-type losses, the contribution of the latter being predominant until the percolation transition. The energy flux density of the incident microwave radiation required to sustain the prescribed heating rate is shown to increase during the microwave heating process from ~20 W/cm$^2$ to >1 kW/cm$^2$ due to increasing reflection. The additional microwave energy input required for the completion of the endothermic oxide decomposition reaction is shown to be significant at the initial stage of the process (below 200 °C).

## 1. Introduction

Microwave processing is a rapidly emerging manufacturing technology that has found new applications in various fields such as sintering, joining, casting, heat treatment, cladding, and drilling. This technology enhances mechanical and functional properties of materials, reduces defects, and offers economic advantages in power and time savings compared to other conventional processes. Microwave processing produces more uniform and homogeneous structures due to hybrid and selective heating. It has found wide application in the food processing industry and the manufacturing industry, with properties like controllable electric field distribution, rapid heating, selective heat deposition, self-limiting reactions, and lower environmental impact [1,2].

Microwave sintering of powder materials has been attracting interest of researchers for several decades. In ceramics, it has been found that the use of microwave heating offers significant advantages from the

* Corresponding author.
*E-mail address:* rybakov@ipfran.ru (K.I. Rybakov).
[1] On Sabbatical leave from Fabrication Technology Department, Advanced Technology and New Materials Research Institute (ATNMRI), City for Scientific Research and Technological Applications (SRTA), New Borg Al-Arab City, P.O.Box: 21934, Alexandria, Egypt.

viewpoint of energy efficiency, process duration, and the properties of the final materials [3–5]. These advantages have been predominantly associated with the ability of ceramic materials to absorb microwave radiation volumetrically due to dielectric losses. In addition to ceramic materials, microwave sintering of powder metals has also been demonstrated, starting with a pioneering work by Roy et al. [6]. Since the beginning of the 21st century, there have been many reports of successful use of microwave heating for the sintering of a broad class of metals and metal-based composites (see, e.g., Refs. [7–13] for a review). Recent research in microwave processing of metals embraces, *inter alia,* an increasing use of microwave sintering for the fabrication of metal matrix composites [14–18], multiphysics simulations [19,20], and microwave-assisted additive manufacturing [21].

Copper is the metal that possesses the highest electrical conductivity. Therefore it has the largest reflection coefficient for the electromagnetic radiation, which makes its microwave sintering a difficult task. However, there have been a number of studies in which copper powders were sintered using microwave heating. Takayama et al. [22] observed an enhancement of the deoxidation reaction in copper powder compacts under microwave heating. Mondal et al. [23] studied the effect of copper particle size and the initial compaction density on the microwave heating and found that finer powders heat faster and reach higher temperatures, and that a lower initial density results in a higher heating rate. Zhu et al. [24] microwave sintered copper powder to a relative density of 97.3 % and demonstrated that the remaining pores concentrated at the edge rather than in the core of the sample. Saitou [25] demonstrated microwave-enhanced low-temperature shrinkage of the copper compacts, which was especially pronounced for fine powders, and determined that the activation energy for sintering was not changed, hence it was the preexponential factor that was responsible for the enhancement. Demirskii and Ragulya [26] investigated microwave sintering of a monolayer of copper particles and found a shift of the shrinkage curves towards low temperatures compared to conventional sintering, which suggested existence of a special mechanism of microwave influence resulting in an increase in the diffusivity. Kumar et al. [27] studied microwave sintering of a copper-based metal matrix composite and observed microwave-enhanced grain boundary diffusion and restricted grain coarsening.

Purposely designed experiments have confirmed that microwave heating can be of a volumetric nature in metal powders [28]. The microwave absorption in metal particles is primarily associated with eddy currents driven by the rotational electric field induced by the alternating magnetic component of the electromagnetic wave field [8,28,29]. In addition, Joule losses of the currents driven directly by the electric component of the field also contribute to absorption, especially at higher (millimeter-wave) frequencies [30].

Electromagnetic radiation is absorbed in a metal particle most efficiently when its size is on the order of the effective penetration depth (skin depth). For the microwave range, this corresponds to a particle size on the order of a micron. Therefore, efficient volumetric microwave absorption in metal powder compacts is only possible when the powder particles are electrically insulated from each other. Rybakov et al. [28] explained the experimentally observed volumetric microwave absorption of metal powders by the presence of non-conductive oxide films on the surface of metal powder particles. Sueyoshi and Honbo [31] demonstrated experimentally that the presence of an oxide film on copper powder particles enhanced its microwave heating. Mahmoud et al. [32] showed that the native thin oxide films on copper metal particles formed under ambient handling conditions had a significant effect on the sintering behavior during high-frequency microwave sintering. In a recent study, Mostovshchikov et al. [33] observed a non-thermal influence of nanosecond microwave pulses on the properties of the oxide films on metal particles, resulting in a decrease of the onset temperature of powder particles oxidation.

There have been a number of studies aimed on direct investigation of oxide films by advanced experimental methods such as using small-angle X-ray scattering (SAXS) and simultaneous wide-angle X-ray scattering (WAXS) measurements to investigate nanostructured and functionalized particles. Quick *in situ* simultaneous SAXS/WAXS measurements were done to measure different disperse particulate systems, such as powders and suspensions as well as aerosol nanoparticles [34]. The information that can be obtained by such methods includes crystal phases, determination of crystal sizes, investigation of crystal phase transformation, determination of primary particle size and size distribution, agglomerate size, surface and mass fractal dimensions describing the roughness of particle surface and the 3D mass-fractal network structures, specific surface area and the thickness of diffuse boundary nanostructured layer on the particle surface. Furthermore, several types of copper oxide thin films ($Cu_2O$, $Cu_4O_3$, and CuO) that were prepared using the reactive magnetron sputtering method were studied using Kelvin probe force microscopy (KPFM) and conductive AFM (C-AFM) [35] where different resistivity values were reported for the different oxides studied. The band gaps of $Cu_2O$, $Cu_4O_3$, and CuO thin films were reported as $2.51 \pm 0.02$ eV, $1.65 \pm 0.1$ eV, and $1.42 \pm 0.01$ eV, respectively, while the resistivity values were $(3.7 \pm 0.3) \times 10^3$ Ω cm, $(1.1 \pm 0.3) \times 10^3$ Ω cm, and $(1.6 \pm 0.6) \times 10^1$ Ω cm, respectively. Moreover, it was found that the $Cu_2O$ film with the largest resistivity had the largest band gap and the least Cu valence state, while the CuO film with the least resistivity had the smallest band gap and the largest Cu valence state.

Other studies had used high-resolution transmission electron microscopy (HRTEM) to investigate the effect of non-uniform copper oxide films formation on the surface of 10 μm-diameter Cu/SnAg microbumps due to copper surface diffusion, around several hundred nm thick. The study was done during tin whisker growth behavior investigation on microbumps under long-term compressive stress [36] where the weak spots of the copper oxide films were found to be a potential place for tin whisker growth.

Copper oxide films produced via a controlled diode laser technique were characterized using different material characterization methods, including TEM, and compared with the film obtained using a thermal copper oxidation process at 300 °C in an infrared oven in normal atmosphere [37]. It was observed that a mixture of $Cu_2O$ and CuO was obtained for all investigated samples, and uneven film thicknesses with different ratios of $Cu_2O$ to CuO were reported for both methods.

In a recent study [38], thin oxide films on the surface of copper powder particles have been investigated using Auger electron spectroscopy (AES) measurements and dual beam focused ion beam scanning electron microscope (FIB/SEM) system where a protective Pt coating with a special stage setup was used to determine the films thickness. The thin oxide films were inhomogeneously covering the copper particle surfaces while their thickness was strongly depending on the particle size. The film thickness was in the range from 22 to 67 nm for 10 μm average particle size (APS) copper particles to 850–1050 nm for the particles of <149 μm in diameter. In addition, copper oxide was also observed inside copper grains and along grain boundaries in smaller amount.

The objective of this paper is to analyze the microwave heating process of copper powder compacts using the recently proposed models for the effective dielectric and magnetic properties of metal powder materials in the microwave range. It is important to mention that the samples used in the current study were the same powders in which the microwave sintering behavior of copper particles was investigated and characterized [32,38]. The results presented below provide information about the evolution of the oxide film on powder particles, the absorption of microwaves in the course of the sintering processes, and the proportion of the electric and magnetic-type losses in the overall absorption.

## 2. Experiment

The microwave sintering experiments [32] were carried out on a 30 GHz gyrotron system for high-temperature microwave processing of materials where different experimental investigations on the sintering behavior of copper metal powders, commonly used in the production of machine components, were done. A commercial gas atomized spherical

copper powder from Alfa Aesar with a particle size of less than 149 μm was used for the preparation of the compacts analyzed in this study. More detailed specifications of this powder were given elsewhere [32,38]. The progress of the 30 GHz microwave sintering process of the cylindrical metal powder compacts, die-pressed under a 5 kN force to a diameter of ~6.4 mm and a height of ~9.5 mm, was investigated at different types of processing gas environments: argon, nitrogen, and forming gas (8 % $H_2$ + 92 % $N_2$). The microwave sintering experiments were carried out at a heating rate of 10 °C/min to a maximum temperature of 1000 °C. The experiments combined both the *in situ* electrical resistance measurements using the four-wire method and the *in situ* dilatometry measurements using a modified dilatometer set-up for monitoring the microwave sintering kinetics as a function of temperature, as shown in Fig. 1. The effects of the processing atmosphere, the particle size and the initial green density of the compacts on the sintering behavior and densification kinetics of the microwave sintered copper compacts were described elsewhere [32]. Table 1 lists the samples data such as particle size, gas used, green and final densities of the investigated samples.

In the course of the experiments, the data on the temperature, shrinkage, and resistance of the samples were recorded with a time step of 5 s. Examples of such records are shown in Fig. 2. These data were used for the analysis described below. Note that an abnormal expansion of copper compacts was observed during the early stages of the microwave sintering process specifically under hydrogen containing gas atmosphere (forming gas, 8 % $H_2$ + 92 % $N_2$).

The structure and properties of the oxide films on copper powder particles were investigated by the following methods: Auger Electron Spectroscopy (AES), dual beam system combining a scanning electron microscope (SEM) and a focused ion beam (FIB) units together (FIB/SEM system), X-ray diffraction (XRD), and carrier gas hot extraction (CGHE) methods, where full details were published in the previous work [38]. The Cu metal particles under investigation were qualitatively characterized using AES measurements, resulting in a rough thickness estimation due to AES method limitation and electron beam induced reduction. The AES analysis was conducted using ultra-high voltage vacuum, 10 keV accelerating voltage, 20 nA current, 24 nm beam size, and sample tilting angle. Depth profiles were also performed using argon ion beam for sputtering/etching, with the analysis conditions adapted for $SiO_2$ standard.

The XRD pattern characterization had revealed the typical face centred cubic (FCC) crystal structure of Cu metal with a lattice parameter of 3.61500 Å and a space group of Fm-3m with no detection of any kind of Cu oxides peaks within the detection limit of XRD technique. XRD was performed on a Seifert C3000 powder diffractometer using $CuK_\alpha$ radiation with 2θ scan range from 5 to 100°.

**Table 1**
Particle size, gas used, green and final densities of the investigated samples.

| Sample ID | Particle size | Gas environment | Green density | Final density |
|---|---|---|---|---|
| S1 | <149 μm | Forming gas (8 % $H_2$ + 92 % $N_2$) | 78.7 % | 83.3 % |
| S2 | <149 μm | Nitrogen | 76.0 % | 79.8 % |
| S3 | <149 μm | Argon | 76.5 % | 84.1 % |

The quantitative characterization of the oxide film was achieved using the dual beam FIB-SEM system and CGHE method. The oxygen content of the as-received Cu powders was found to have a mean value of around 0.575 wt% with a detection limit of 0.006 wt% using CGHE. The CGHE measurement was done using a commercial oxygen/nitrogen analyzer TC600 (LECO). The analyzer was calibrated with the certified standard JK 47 and verified with a copper standard from ELTRA. The standards and samples were weighed with a mass range of 5–30 mg, with a weighing accuracy of ±0.002 mg, and placed in a high temperature graphite crucible for outgassing. The $CO_2$ and CO gases were then swept out by helium as an inert gas carrier and measured via non-dispersive infrared photometry (NDIR).

The thickness of the oxide film was quantitatively characterized with an improved accuracy using the dual beam FIB-SEM system. A novel setup was used in FIB/SEM measurements where Pt-coated Cu particles were sliced via *in situ* FIB sectioning at 0° stage tilt and directly followed by oxide film thickness characterization using SEM imaging at 36° stage tilt to avoid any stage tilt correction with best resolution when using different detection modes. The oxide film was found to be inhomogeneously covering the particle surface, and its thickness strongly depended on the particle size. The dual system's working voltage conditions were: high voltage SEM 0.2 kV–30 kV and high-voltage FIB 0.2 kV–30 kV, with electron beam resolutions of 1 nm at 15 and 30 kV.

## 3. Theory

The experimental data recorded in the microwave sintering processes are analyzed below using a number of previously proposed theoretical models.

The materials considered in this work are inhomogeneous, i.e., consisting of several phases: solid copper, solid copper oxide, and void space in the pores between the particles. The scale length of non-uniformities (nanometers to microns) is very small compared to most physical scale lengths that are relevant to the description of the

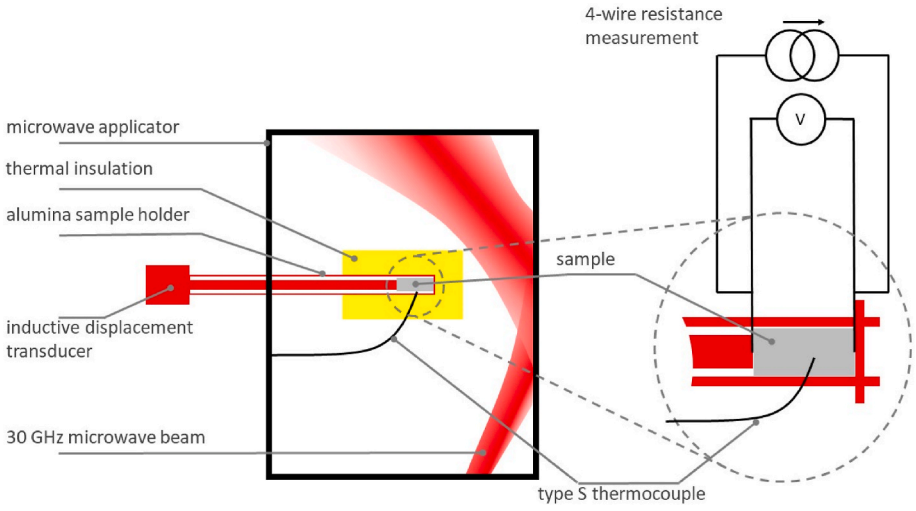


**Fig. 1.** Schematic of the 30 GHz gyrotron microwave system showing *in situ* measurements of linear shrinkage in combination with resistance measurements, adapted from Ref. [32].

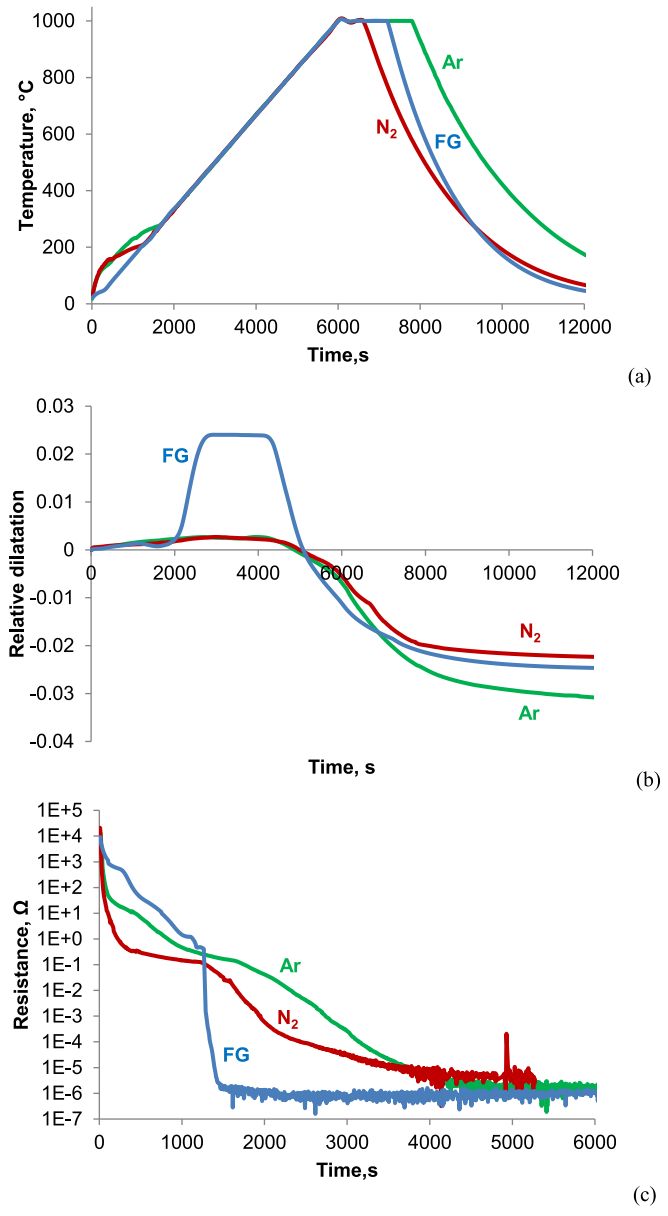


**Fig. 2.** Temperature (a), relative dilatation (b), and resistance (c) of copper powder samples recorded during the microwave sintering experiments carried out in three different gas environments: argon (Ar), nitrogen ($N_2$), and forming gas (FG).

microwave heating process, such as the dimensions of the sample and the electromagnetic wavelength. In this case the effective macroscopic properties of an inhomogeneous material can be obtained by methods based on averaging. The effective properties are generally determined by the properties of each constituent material, their relative concentration, shape and size distributions of the particles, *etc*. For approximate description of the macroscopic properties of inhomogeneous materials, various models of host media with inclusions (also known as mixing laws) that allow analytical implementation of the averaging procedure have been proposed (see, e.g., Refs. [39,40]). Their applicability is determined experimentally, and usually it is limited to a certain range of the inclusion concentration. Among these models, widely used are the so-called effective medium approximations, originally proposed almost a century ago [41], in which all constituent materials are viewed as inclusions in the "effective" host medium with the originally unknown properties that are determined as a result of the averaging procedure. These models are symmetric with regard to all constituents and provide reasonable agreement to experiment in a broad range of their concentration.

In this work, we use the effective medium models in which copper particles and void space are modeled as spherical inclusions, and the oxide film forms a spherical shell around each copper inclusion. The effective electrical conductivity of the compacted copper powder $\sigma_{\text{eff}}$ is determined from the equation [42]

$$2\beta\sigma_{\text{eff}}^2 + \left[\beta\sigma_g(3C_s \quad 2) + \alpha\sigma_i(1 \quad 3C_s)\right]\sigma_{\text{eff}} \quad \alpha\sigma_i\sigma_g = 0, \tag{1}$$

where $C_s$ the relative concentration of solid (metal + oxide) in the porous material, $\alpha = (2\sigma_i + \sigma_m)(b/a)^3 + 2(\sigma_m \quad \sigma_i)$, $\beta = (2\sigma_i + \sigma_m)(b/a)^3 + \sigma_i \quad \sigma_m$, $a$ is the radius of metal powder particle without the oxide film, $b$ is the outer radius of the powder particle with the oxide film, $\sigma_m$ is the conductivity of metal, $\sigma_i$ is the conductivity of the insulating oxide material (both conductivities are temperature-dependent), and $\sigma_g$ is the conductivity of the gas contained in the pores. Based on Eq. (1), the indicative thickness of the oxide film can be determined from the *in situ* measurements of the resistance of the cylindrical compacted powder samples during the microwave sintering process.

The equation for the effective complex dielectric permittivity $\varepsilon_{\text{eff}}$ of the powder material described above is obtained from the model considering the wave structure of the electromagnetic field in the individual particles [30]. This model adequately describes good electrical conductors at higher microwave frequencies, such as copper at 30 GHz:

$$\begin{aligned} &2w_1w_2\varepsilon_{\text{eff}}^3 + [6C_s\varepsilon_i(w_2q_7 \quad w_1q_8) + (3C_s \quad 2)w_1w_2 + 2(w_1w_4 + w_2w_3)]\varepsilon_{\text{eff}}^2 \\ &+[3C_s\varepsilon_i(2w_4q_7 + w_2q_7 \quad 2w_3q_8 \quad w_1q_8) + (3C_s \quad 2)(w_1w_4 + w_2w_3) \\ &\quad + 2w_3w_4]\varepsilon_{\text{eff}} \\ &+ 3C_s\varepsilon_i(w_4q_7 \quad w_3q_8) + (3C_s \quad 2)w_3w_4 = 0, \end{aligned} \tag{2}$$

where

$$w_1 = q_9 + \frac{\varepsilon_i q_2 q_4 \quad \varepsilon_c q_1 q_5}{\varepsilon_i q_3 q_4 + \varepsilon_c q_1 q_6} q_{10},$$

$$w_2 = \frac{\varepsilon_i q_3 q_4 + \varepsilon_c q_1 q_6}{\varepsilon_i q_2 q_4 \quad \varepsilon_c q_1 q_5} q_9 + q_{10},$$

$$w_3 = \varepsilon_i\left(\frac{\varepsilon_i q_2 q_4 \quad \varepsilon_c q_1 q_5}{\varepsilon_i q_3 q_4 + \varepsilon_c q_1 q_6} q_8 \quad q_7\right),$$

$$w_4 = \varepsilon_i\left(q_8 \quad \frac{\varepsilon_i q_3 q_4 + \varepsilon_c q_1 q_6}{\varepsilon_i q_2 q_4 \quad \varepsilon_c q_1 q_5} q_7\right),$$

$$q_1 = \frac{k_m \cos k_m a}{a} \quad \frac{\sin k_m a}{a^2},$$

$$q_2 = \frac{k_i \cos k_i a}{a} \quad \frac{\sin k_i a}{a^2},$$

$$q_3 = \frac{k_i \sin k_i a}{a} + \frac{\cos k_i a}{a^2},$$

$$q_4 = \frac{k_m^2 \sin k_m a}{a} + \frac{k_m \cos k_m a}{a^2} \quad \frac{\sin k_m a}{a^3},$$

$$q_5 = \frac{k_i^2 \sin k_i a}{a} + \frac{k_i \cos k_i a}{a^2} \quad \frac{\sin k_i a}{a^3},$$

$$q_6 = \frac{k_i^2 \cos k_i a}{a} \quad \frac{k_i \sin k_i a}{a^2} \quad \frac{\cos k_i a}{a^3},$$

$$q_7 = \frac{k_i \cos k_i b}{b^2} \quad \frac{\sin k_i b}{b^3},$$

$$q_8 = \frac{k_i \sin k_i b}{b^2} + \frac{\cos k_i b}{b^3},$$

$$q_9 = \frac{k_i^2 \sin k_i b}{b} + \frac{k_i \cos k_i b}{b^2} \quad \frac{\sin k_i b}{b^3},$$

$$q_{10} = \frac{k_i^2 \cos k_i b}{b} \quad \frac{k_i \sin k_i b}{b^2} \quad \frac{\cos k_i b}{b^3},$$

$k_i = k_0\sqrt{\varepsilon_i}$ and $k_m = k_0\sqrt{\varepsilon_m}$ are the wavenumbers in the dielectric and metal, respectively, $k_0 = \omega/c$ is the vacuum wavenumber, $\omega = 2\pi f$ is the

cyclic frequency of microwaves, $c$ is the velocity of light, $\varepsilon_m \approx i\sigma_m/\varepsilon_0\omega$ is the dielectric permittivity of the metal, $i$ is the imaginary unit, $\varepsilon_i = \varepsilon_i' + i\sigma_i/\varepsilon_0\omega$ is the dielectric permittivity of the oxide, and $\varepsilon_0$ is the electric constant.

The effective complex magnetic permeability $\mu_{\text{eff}}$ of the compacted metal powder is obtained from the equation [43]

$$2(\xi + k_m^2 a^2)\mu_{\text{eff}}^2 + [\xi(9C_m \quad 4) + k_m^2 a^2(3C_m \quad 2)]\mu_{\text{eff}} + 2\xi = 0, \tag{3}$$

where $\xi = k_m a \cot k_m a \quad 1$, and $C_m$ is the relative volumetric concentration of metal in the compact.

The absorbed microwave power $p$, per unit volume, is calculated within a simple model of a uniform slab of the powder material with the effective properties (2) and (3), irradiated normally by a plane, linearly polarized electromagnetic wave. The thickness of the slab is taken equal to the height of the cylindrical sample, $h$. It is instructive to calculate separately the contribution of the dielectric and magnetic-type losses, $p_E$ and $p_M$, that are proportional to the imaginary parts of the effective dielectric permittivity $\varepsilon''_{\text{eff}}$ and magnetic permeability $\mu''_{\text{eff}}$, respectively:

$$p(z) = p_E(z) + p_M(z) = \frac{1}{2}\varepsilon''_{\text{eff}}\varepsilon_0\omega|E(z)|^2 + \frac{1}{2}\mu''_{\text{eff}}\mu_0\omega|H(z)|^2, \tag{4}$$

where $z$ is the propagation direction of the electromagnetic wave (across the slab) and $\mu_0 = 1/(c^2\varepsilon_0)$ is the magnetic constant. The complex amplitudes of the electric and magnetic field in the slab $E(z)$ and $H(z)$ are:

$$\begin{aligned} E(z) &= E_0\left(Be^{ikz} + Ce^{-ikz}\right), \\ H(z) &= H_0\left(Be^{ikz} \quad Ce^{-ikz}\right)/\zeta, \end{aligned} \tag{5}$$

where $\zeta = \sqrt{\mu_{\text{eff}}/\varepsilon_{\text{eff}}}$ is the impedance of the material, $k = k_0\sqrt{\varepsilon_{\text{eff}}\mu_{\text{eff}}}$ is the wavenumber in the material, $E_0$ and $H_0$ are the amplitudes of the electric and magnetic field, respectively, in the incident wave. The amplitudes $E_0$ and $H_0$ are interrelated as $E_0 = \zeta_0 H_0$, where $\zeta_0 = \sqrt{\mu_0/\varepsilon_0}$ is the so-called impedance of free space. The coefficients $B$ and $C$ are determined from the boundary conditions:

$$\begin{aligned} B &= \frac{(1+\zeta)(\cos kh \quad i\sin kh)}{2\cos kh \quad i\left(\frac{1}{\zeta} + \zeta\right)\sin kh}, \\ C &= \frac{(1 \quad \zeta)(\cos kh + i\sin kh)}{2\cos kh \quad i\left(\frac{1}{\zeta} + \zeta\right)\sin kh}. \end{aligned} \tag{6}$$

The power absorbed in the powder material, per unit area of the slab, can be presented as a sum of the dielectric and magnetic-type losses:

$$P = P_E + P_M, \tag{7}$$

$$P_E = \int_0^h p_E(z)dz = \frac{1}{2}\varepsilon''_{\text{eff}}\varepsilon_0\omega E_0^2(V + W),$$

$$P_M = \int_0^h p_M(z)dz = \frac{1}{2}\mu''_{\text{eff}}\mu_0\omega\frac{E_0^2}{\varsigma_0^2|\varsigma|^2}(V \quad W),$$

where $V = \left[|C|^2\left(e^{2k''h} \quad 1\right) \quad |B|^2\left(e^{\ 2k''h} \quad 1\right)\right]/(2k'')$, $W = 2\sin k'h[(B'C' + B''C'')\cos k'h + (B'C'' \quad B''C')\sin k'h]/k'$, primes and double primes refer to the real and imaginary parts, respectively.

The absorbed power (7) calculated as described above, supplemented with an energy balance equation, can be readily used to simulate microwave heating of compacted metal powders. Examples of such calculations performed for the microwave sintering of titanium and nickel powders can be found in Ref. [42]. Shown in Fig. 3 are examples of the temperature curves for the microwave heating of copper powder by a fixed intensity of 30 GHz radiation, calculated for three different values of the oxide film thickness under an assumption that the only heat loss channel is thermal radiation. It can be seen that the temperature growth rate depends strongly on the thickness of the oxide layer due to its influence on the microwave absorption of the powder material. In the particular example shown in Fig. 3, the total fraction of the incident power absorbed in the slab of copper powder during the microwave heating process was on the order of 0.6 % for an oxide film thickness of 10 nm, 2 % for 100 nm, and 6 % for 1 μm.

The problem addressed in the remainder of this paper is of an inverse nature to the straightforward approach illustrated by Fig. 3. First, the oxide film thickness is derived from the *in situ* resistance measurements on copper compacts. Then the effective dielectric properties and the microwave absorption efficiency are calculated, and finally the evolution of the microwave power needed to sustain the experimentally implemented temperature growth is simulated.

## 4. Results and discussion

### 4.1. Thickness of the oxide film on metal particles

Using the recorded data on the resistance of the copper compacts during microwave sintering, the indicative thickness of the oxide film on the surface of copper particles was determined based on the effective medium approximation for the electrical conductivity (Eq. (1)). For this purpose, the effective conductivity was expressed via the measured resistance $R$ as

$$\sigma_{\text{eff}} = \frac{4h}{\pi d^2 R}, \tag{8}$$

where $h$ and $d$ are the height and diameter of the cylindrical sample (which change during the process in accordance with the sample dilatation data). The oxide film thickness, $b - a$, was then expressed from Eq. (1), neglecting the conductivity of gas in the pores, as

$$b \quad a = a\left\{\sqrt[3]{\frac{2(\sigma_m \quad \sigma_i)[\sigma_{\text{eff}} + (3C_s \quad 1)\sigma_i]}{(\sigma_m + 2\sigma_i)[2\sigma_{\text{eff}} \quad (3C_s \quad 1)\sigma_i]}} \quad 1\right\}. \tag{9}$$

The temperature dependencies of the conductivities of copper, $\sigma_m$, and of copper oxide, $\sigma_i$, were taken from Refs. [44,45], respectively. The relative density of the solid material in the compact, $C_s$, was calculated from the dilatation data.

The calculated indicative thickness of the oxide film is plotted in Fig. 4 as a function of temperature for three microwave sintering processes carried out at a heating rate of 10 °C/min in different gas

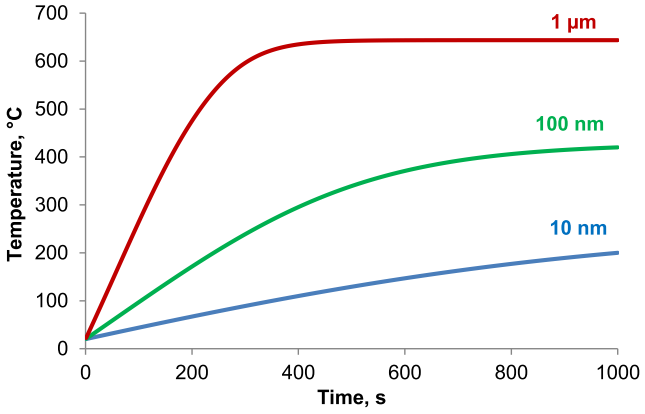


**Fig. 3.** Temperature vs. time curves calculated for the heating of a slab of compacted copper powder (particle radius 22 μm, relative density 76 %, slab thickness 9.5 mm) by 30 GHz microwave radiation with a fixed intensity of 100 W/cm$^2$ for three different values of the thickness of oxide film on powder particles.

environments: argon, nitrogen, and forming gas. The characteristic radius of the copper powder particles, *a*, was taken equal to 22 μm. This is close to the median particle radius because from the particle size distribution of this powder [32] it is known that 53.8 % of all particles have a size of less than 44 μm.

According to the results of the microstructure studies accomplished with the same copper powder [38], the characteristic initial thickness of the oxide film on the powder particles was 850–1050 nm. The calculation results shown in Fig. 4 give an about one order of magnitude higher indicative thickness at the start of the process, which probably reflects the excess resistance that stems from surface roughness of the particles resulting in poor electrical contact between them. After a sharp initial decline, probably associated with the suppression of the surface roughness, the indicative thickness acquires the same order of magnitude, ~1 μm, as the experimentally measured value. Then the calculated thickness of the oxide film decreases gradually as the temperature increases, reflecting the incremental decomposition of the copper oxide. The film thickness is about one order of magnitude lower in the case of nitrogen environment than in argon, which suggests faster decomposition of the oxide. This could be related to the reaction of nitrogen with oxygen under the effect of possible microwave arcing and electrical discharges during sintering [46]. This reaction is well documented and known as the Birkeland–Eyde process where an endothermic reaction between nitrogen and oxygen is taking place in presence of an electric arc discharges [47,48], as per the reaction equations below:

$$\begin{aligned} &N_2 + O_2 \rightarrow 2NO \\ &2NO + O_2 \rightarrow 2NO_2 \end{aligned} \quad (10)$$

An indicative thickness of the oxide film on the order of 0.1 nm, which corresponds to a molecular monolayer, is reached at a temperature of about 290 °C for nitrogen and 440 °C for argon. Further decrease of the calculated indicative thickness is physically meaningless. Beyond this point, the decreasing resistance of the compacted copper powder sample probably reflects the progress of the neck growth between copper particles in the course of sintering.

In the case of forming gas environment, the evolution of the calculated indicative film thickness is initially similar to the cases of argon and nitrogen. However, at a temperature of about 210 °C the film thickness drops down very sharply to physically unmeaningful values, well below 0.1 nm, This may suggest that in the presence of hydrogen, copper oxide is reduced to metal completely at this point, as shown previously [32]. Therefore, the data obtained in the experiments carried out in forming gas are not used for the calculations described in the remainder of this paper.

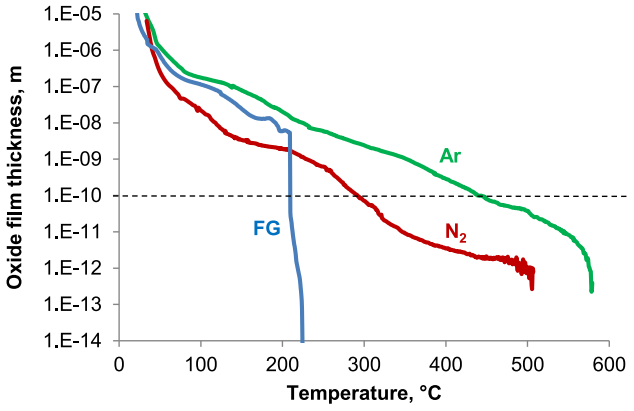


**Fig. 4.** The indicative thickness of the oxide film on copper powder particles calculated from the sample resistance data as a function of temperature for three microwave sintering processes carried out in different gas environments: argon (Ar), nitrogen ($N_2$), and forming gas (FG).

### 4.2. *Effective dielectric permittivity and magnetic permeability*

With the thickness of the oxide film determined in the previous section, the effective dielectric permittivity and magnetic permeability can be readily calculated using Eqs. (2) and (3), respectively. The calculation results obtained for the microwave frequency of 30 GHz are shown in Fig. 5.

It can be seen from Fig. 5a that the effective dielectric properties of the copper powder exhibit a typical percolation behavior [49]: the imaginary part of the effective complex dielectric permittivity undergoes a sharp growth by several orders of magnitude as the material evolves from insulating to conductive due to decomposition of the oxide films of the particles. The real part of the effective complex dielectric permittivity exhibits a maximum at which its magnitude is approximately equal to the imaginary part, and then decreases rapidly. High value of the real part can be explained by the formation of a network of microcapacitors between the neighboring copper particles separated by very thin dielectric (oxide) layers in which the electric field is locally concentrated [49,50]. With further decrease in the thickness of the oxide film the electric field is suppressed due to increasing effective high-frequency conductivity of the material, which explains the drop in the real part of the dielectric permittivity [51].

Both the real and imaginary parts of the effective complex magnetic permeability of the copper powder (Fig. 5b) are below 0.1 in the entire range of calculation. This apparent diamagnetism originates from the high-frequency magnetization produced by the eddy currents that arise in the particles in response to the microwave field.

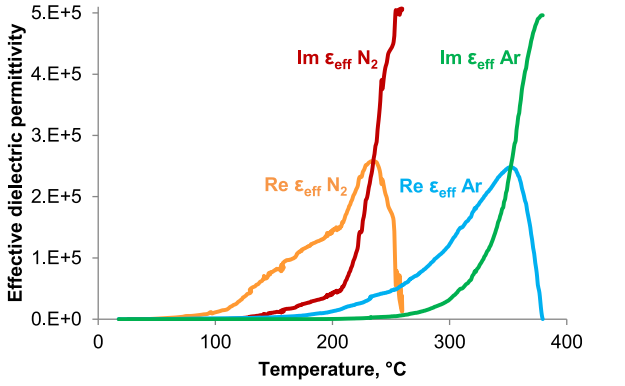


(a)

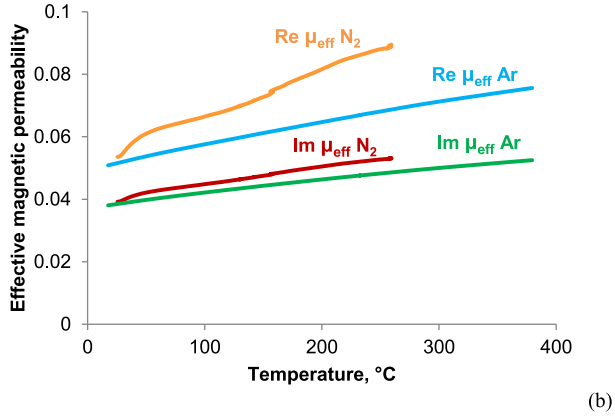


(b)

**Fig. 5.** The effective complex dielectric permittivity, $\varepsilon_{eff}$ (a), and magnetic permeability, $\mu_{eff}$ (b), of the compacted copper powder with oxide films on the particles during the 30 GHz microwave heating processes carried out in different gas environments: argon (Ar) and nitrogen ($N_2$).

### 4.3. Microwave absorption efficiency

It is instructive to investigate the microwave absorption efficiency of the copper powder during the microwave sintering process. It can be expected that the growing conductivity of the powder material gives rise to an increasing reflection of microwaves and thereby to a decreasing efficiency of absorption.

Shown in Fig. 6 are the plots of the relative absorption efficiency of the 30 GHz microwave radiation in the slab of copper powder material. To calculate the relative efficiency, the power absorbed per unit area of the slab is normalized by the energy flux in the incident electromagnetic wave, $P_0 = E_0 H_0 = E_0^2/\zeta_0$. The contributions of the dielectric and magnetic types of losses, $P_e/P_0$ and $P_m/P_0$, are plotted separately.

It can be seen that the absorption due to magnetic-type losses (associated with eddy currents in the conductive powder particles) is prevailing during the initial stage of the microwave heating process. At the start of the process, the relative absorption efficiency is about 14 % in nitrogen and 22 % in argon. As the effective dielectric permittivity of the powder material grows (see Fig. 5), most of the microwaves get reflected, and the absorption efficiency decreases to less than 1 %.

The dielectric-type losses arise from the Joule losses of the currents driven in the metal powder particles directly by the electric component of the field, and also from the dielectric losses in the oxide films. Their contribution into the absorption efficiency is on the order of 0.1 % throughout the process. As seen from Fig. 6, at higher temperatures the contribution of the magnetic-type losses becomes lower than the contribution of the dielectric losses. However, by that time the microwave radiation is almost fully (~99.8 %) reflected from the copper compact.

### 4.4. Microwave power required to implement the heating process

Using the experimentally recorded temperature-time evolution of the sample, it is easy to calculate the power needed to raise the temperature of the sample at each time step. Then, using the absorption efficiency calculated above in Section 4.3, it is possible to obtain the evolution of the microwave energy flux density incident on the slab of copper powder material which would be necessary to sustain the temperature-time schedule. The results of such a calculation, taking into account both the changes in the thickness of the oxide film and the dilatation of the samples, are shown in Fig. 7 for the processes carried out in nitrogen and argon environments.

It can be seen from Fig. 7 that the required microwave energy flux density grows as the efficiency of microwave absorption decreases in the course of the process, as discussed above. For the case of heating in argon, the required microwave energy flux density exceeds 1 kW/cm$^2$ at a temperature of about 400 °C. For the case of heating in nitrogen, the required energy flux density grows even faster. Obviously, in practical terms these prohibitively high energy flux density levels mean that the microwave heating process cannot be continued beyond this point if only direct microwave absorption in the copper powder is employed and no additional absorbing materials (susceptors) are used.

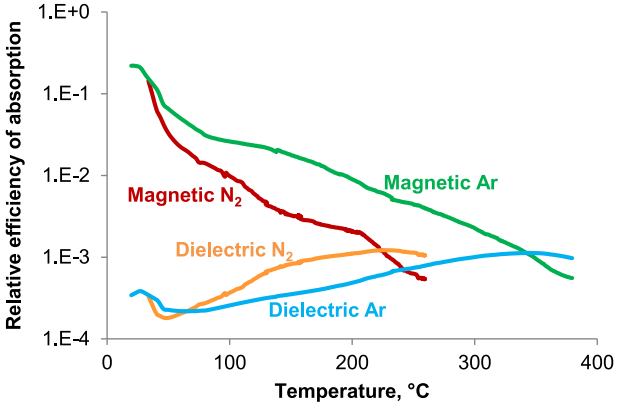


**Fig. 6.** Relative efficiency of 30 GHz microwave absorption in a slab of compacted copper powder due to dielectric and magnetic-type losses during the microwave heating processes carried out in different gas environments: argon (Ar) and nitrogen ($N_2$).

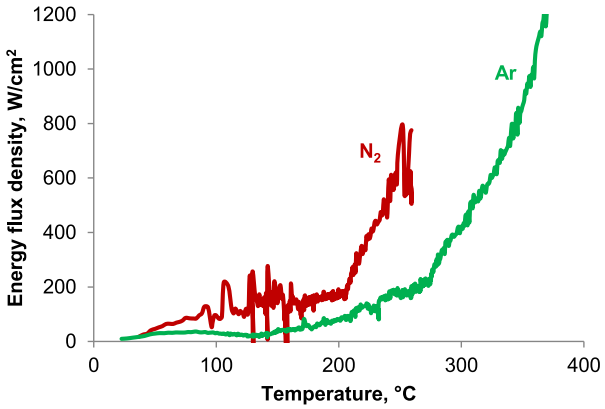


**Fig. 7.** The evolution of the 30 GHz microwave energy flux density incident on the slab of copper powder material required to sustain the experimentally recorded temperature-time schedule of the microwave sintering processes carried out in different gas environments: argon (Ar) and nitrogen ($N_2$).

This result is in agreement with an experiment on the 24 GHz microwave heating of different metal powders using two thermocouples measuring the temperature in the center and at the periphery of the compact [28]. In the case of copper powder no difference was observed between the temperatures measured by the two thermocouples, which suggests that there was no volumetric heating and no microwave absorption. As opposed to that, volumetric heating was indeed observed in Ref. [28] in the case of iron powder (iron has an about six times lower conductivity than copper).

In the experimental configuration described in Ref. [32], the copper sample could be heated indirectly from the microwave-heated ceramic parts that were present in the system (for example, the ceramic rod of the dilatometer, surrounded along with the sample by the heat-insulating material). An increase in the 30 GHz microwave absorptivity of the ceramic rod or the heat-insulating material, occurring at an intermediate temperature, would result in the decrease in the microwave power which was indeed observed in the experiments described in Ref. [32].

When the oxide film is being decomposed during the heating process, the absorbed microwave power is spent not only on the increase of the temperature of the sample, but also on the enthalpy of the decomposition reaction, which in the case of CuO is equal to 157 kJ/mol [52]. The contribution of decomposition should be significant at the initial stage of the process, when the oxide film thickness is considerable, and decrease as the thickness of the film goes down to the nanometer range. This is illustrated by Fig. 8, in which the microwave energy flux density required to sustain the temperature-time schedule calculated taking into account the contribution of decomposition. It can be seen that at the initial stage a highly significant microwave energy flux density would be required to decompose the oxide film with a rather high indicative thickness as determined by calculation (see Fig. 4). However, as mentioned above, there are certain reservations regarding these estimates, since the high value of the indicative thickness may originate from poor contact between particles due to significant surface roughness. Yet, it can be seen from Fig. 8 that the contribution of decomposition becomes negligible at a temperature of about 200 °C, and from

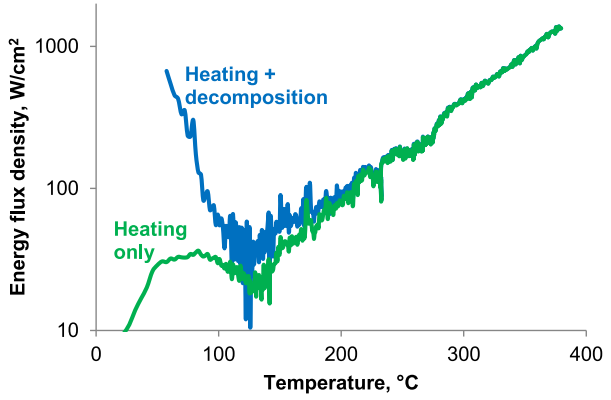


**Fig. 8.** The microwave energy flux density required to carry out the microwave heating process (in argon environment), calculated taking into account the enthalpy of the copper oxide decomposition reaction and without the contribution of decomposition.

this point almost the entire absorbed microwave power is spent on increasing the internal energy of the material.

## 5. Conclusion

The microwave heating of copper powder with oxide films on the surface of particles has been analyzed by numerical simulation based on the data from actual experiments. The indicative thickness of the oxide films has been determined from the resistivity data using an effective medium approximation for spherical conductive particles with partially insulating concentric shells. The thickness decreases in the course of the microwave heating process due to decomposition of the oxide, which is influenced by the gas environment.

The effective complex dielectric permittivity and magnetic permeability of the copper powder have been calculated using the recently proposed effective medium models for the respective properties of metal powders in the microwave range. The calculation is based on the obtained indicative thickness of the oxide films on the surface of powder particles. The effective dielectric permittivity exhibits a pronounced percolation transition at 210–250 °C when microwave heating is carried out in nitrogen and at 330–375 °C – in argon. Both the real and imaginary parts of the effective magnetic permeability increase with temperature, not exceeding 0.1 in the temperature range of simulation.

The efficiency of absorption of the incident 30 GHz microwave radiation in a slab of the copper powder has been calculated based on the solution of the electromagnetic problem using the obtained effective dielectric and magnetic properties. In the beginning of the process the magnetic-type losses are almost entirely responsible for the heating. However, the efficiency of the magnetic-type absorption decreases with temperature and eventually becomes comparable to the electric-type losses. This occurs at a temperature of 220 °C in nitrogen and at 340 °C in argon, i.e., within the temperature range of the percolation transition.

The energy flux density of the incident microwave radiation required to sustain the heating schedule implemented in the experiment has been assessed. It is demonstrated that the decrease in the absorption efficiency dictates an increase in the required energy flux density with temperature. Due to increased reflection, the required energy flux density reaches prohibitively high values, on the order of 1 kW/cm$^2$, at temperatures not exceeding 400 °C. Additional microwave energy is required at lower temperatures (<200 °C) for the completion of the endothermic oxide decomposition reaction.

The results obtained in this study provide physical grounds for an analysis of microwave heating and sintering of metal powders. A simple self-consistent model is presented that links the properties of the oxide film on powder particles, including the kinetics of its decomposition, the structure of the electromagnetic field, the microwave radiation absorption and reflection from the powder material, the contribution of magnetic- and electric-type losses into the absorption, and the evolution of temperature due to direct microwave heating. It is demonstrated that efficient volumetric microwave heating is contingent upon the presence of oxide films on metal powder particles. The knowledge generated using the presented model advances the understanding of the microwave sintering of metals and provides information that may influence the design considerations in developing microwave processing systems.

## Funding

The numerical study of the microwave sintering of a composite material comprising oxide films on metal powder particles was supported by Russian Science Foundation (grant No. 23-19-00363).

## CRediT authorship contribution statement

**K.I. Rybakov:** Writing – original draft, Software, Formal analysis, Conceptualization. **M.M. Mahmoud:** Writing – review & editing, Methodology, Investigation, Data curation, Conceptualization. **G. Link:** Writing – review & editing, Resources, Methodology, Investigation, Data curation.

## Declaration of competing interest

The authors declare that they have no known competing financial interests or personal relationships that could have appeared to influence the work reported in this paper.

## Data availability

Data will be made available on request.

## References

[1] D.E. Clark, W.H. Sutton, Microwave processing of materials, Annu. Rev. Mater. Sci. 26 (1996) 299–331, https://doi.org/10.1146/annurev.ms.26.080196.001503.
[2] Yu.V. Bykov, K.I. Rybakov, V.E. Semenov, High-temperature microwave processing of materials, J. Phys. D Appl. Phys. 34 (2001) R55–R75, https://doi.org/10.1088/0022-3727/34/13/201.
[3] D.E. Clark, D.C. Folz, C.E. Folgar, M.M. Mahmoud (Eds.), Microwave Solutions for Ceramic Engineers, American Ceramic Society, Westerville, 2005.
[4] M. Oghbaei, O. Mirzaee, Microwave versus conventional sintering: a review of fundamentals, advantages and applications, J. Alloys Compd. 494 (2010) 175–189, https://doi.org/10.1016/j.jallcom.2010.01.068.
[5] K.I. Rybakov, E.A. Olevsky, E.V. Krikun, Microwave sintering – fundamentals and modeling, J. Am. Ceram. Soc. 96 (2013) 1003–1020, https://doi.org/10.1111/jace.12278.
[6] R. Roy, D. Agrawal, J. Cheng, S. Gedevanishvili, Full sintering of powdered-metal bodies in a microwave field, Nature 399 (1999) 668–670, https://doi.org/10.1038/21390.
[7] M. Gupta, W.L.E. Wong, Microwaves and Metals, Wiley, Singapore, 2007.
[8] N. Yoshikawa, Fundamentals and applications of microwave heating of metals, J. Microw. Power Electromagn. Energy 44 (2010) 4–13, https://doi.org/10.1080/08327823.2010.11689772.
[9] D. Agrawal, Microwave sintering of metal powders, in: I. Chang, Y. Zhao (Eds.), Advances in Powder Metallurgy (Woodhead Publishing Series in Metals and Surface Engineering), Woodhead Publishing, Sawston, 2013, pp. 361–379, https://doi.org/10.1533/9780857098900.3.361.
[10] R.R. Mishra, A.K. Sharma, A review of research trends in microwave processing of metal-based materials and opportunities in microwave metal casting, Crit. Rev. Solid State Mater. Sci. 41 (2016) 217–255, https://doi.org/10.1080/10408436.2016.1142421.
[11] J. Sun, W. Wang, Q. Yue, Review on microwave-matter interaction fundamentals and efficient microwave-associated heating strategies, Materials 9 (2016) 231, https://doi.org/10.3390/ma9040231.
[12] R.V. Batienkov, A.N. Bol'shakova, A.A. Khudnev, Microwave sintering of metal powder materials (review),, Metallurgist 65 (2022) 1163–1173, https://doi.org/10.1007/s11015-022-01260-y.

[13] U. Gautam, M.E. Asgar, K. Singh, A review on materials processing using microwave radiation, Mater. Today: Proc. 78 (2023) 426–431, https://doi.org/10.1016/j.matpr.2022.10.249.
[14] S.A.A. Alem, R. Latifi, S. Angizi, F. Hassanaghaei, M. Aghaahmadi, E. Ghasali, M. Rajabi, Microwave sintering of ceramic reinforced metal matrix composites and their properties: a review, Mater. Manuf. Process. 35 (2020) 303–327, https://doi.org/10.1080/10426914.2020.1718698.
[15] V.R. Malik, P.A. Bajakke, K.K. Saxena, A. Lakshmikanthan, A.S. Deshpande, S. Mabuwa, V. Masomi, Energy-efficient method for developing in-situ Al-Cu metal matrix composites using microwave sintering and friction stir processing, Mater. Res. Express 9 (2022) 066507, https://doi.org/10.1088/2053-1591/ac7638.
[16] P. Balasundar, S. Senthil, P. Narayanasamy, T. Ramkumar, Mechanical, thermal, electrical, and corrosion properties of microwave-sintered Ti-0.8Ni-0.3Mo/TiB composites, Phys. Scripta 98 (2023) 065954, https://doi.org/10.1088/1402-4896/acd6c5.
[17] D.V. Dudina, K. Georgarakis, E.A. Olevsky, Progress in aluminium and magnesium matrix composites obtained by spark plasma, microwave and induction sintering, Int. Mater. Rev. 68 (2023) 225–246, https://doi.org/10.1080/09506608.2022.2077029.
[18] A. Shakil, R.K. Gautam, U.S. Rao, Characterisation of rapid microwave-sintered Mg/MgO composite, Trans. Indian Inst. Met. 76 (2023) 749–756, https://doi.org/10.1007/s12666-022-02772-6.
[19] C. Manière, G. Lee, T. Zahrah, E.A. Olevsky, Microwave flash sintering of metal powders: from experimental evidence to multiphysics simulation, Acta Mater. 147 (2018) 24–34, https://doi.org/10.1016/j.actamat.2018.01.017.
[20] Y. Li, Y. Cheng, Z. Jiang, Z. Wang, J. Yuan, Microwave sintering of Ti(C,N)-based cermets: study of the magnetic effect on metal phase, Mater. Chem. Phys. 313 (2024) 128717, https://doi.org/10.1016/j.matchemphys.2023.128717.
[21] A. Goulas, T. Whittaker, G. Chi-Tangyie, I.M. Reaney, D. Engstrøm, W. Whittow, B. Vaidhyanathan, Multi-material additive manufacture and microwave-assisted sintering of a metal/ceramic metamaterial antenna structure, Appl. Mater. Today 33 (2023) 101878, https://doi.org/10.1016/j.apmt.2023.101878.
[22] S. Takayama, Y. Saito, M. Sato, T. Nagasaka, T. Muroga, Y. Ninomiya, Sintering behavior of metal powders involving microwave-enhanced chemical reaction, Jpn. J. Appl. Phys. 45 (2006) 1816–1822, https://doi.org/10.1143/JJAP.45.1816.
[23] A. Mondal, D. Agrawal, A. Upadhyaya, Microwave heating of pure copper powder with varying particle size and porosity, J. Microw. Power Electromagn. Energy 43 (2008) 5–10, https://doi.org/10.1080/08327823.2008.11688599.
[24] F.-X. Zhu, J.-H. Yi, Y.-D. Peng, Sintering response of copper powder metal compact in microwave field, Zhongnan Daxue Xuebao (Ziran Kexue Ban), J. Cent. South Univ. (Science and Technology) 40 (2009) 106–111.
[25] K. Saitou, Microwave sintering of iron, cobalt, nickel, copper and stainless steel powders, Scripta Mater. 54 (2006) 875–879, https://doi.org/10.1016/j.scriptamat.2005.11.006.
[26] D.N. Demirskii, A.V. Ragulya, Initial kinetics of microwave sintering of copper, Powder Metall. Met. Ceram. 49 (2010) 147–152, https://doi.org/10.1007/s11106-010-9214-8.
[27] V. Kumar, G. Yadav, P. Gupta, Structural and mechanical behavior of copper-TiC-graphite hybrid metal matrix composites fabricated by microwave sintering technique, ECS J. Solid State Sci. Technol. 12 (2023) 047001, https://doi.org/10.1149/2162-8777/acca48.
[28] K.I. Rybakov, V.E. Semenov, S.V. Egorov, A.G. Eremeev, I.V. Plotnikov, Yu. V. Bykov, Microwave heating of conductive powder materials, J. Appl. Phys. 99 (2006) 023506, https://doi.org/10.1063/1.2159078.
[29] J. Cheng, R. Roy, D. Agrawal, Experimental proof of major role of magnetic field losses in microwave heating of metal and metallic composites, J. Mater. Sci. Lett. 20 (2001) 1561–1563, https://doi.org/10.1023/A:1017900214477.
[30] K.I. Rybakov, V.E. Semenov, Effective microwave dielectric properties of ensembles of spherical metal particles, IEEE Trans. Microw. Theor. Tech. 65 (2017) 1479–1487, https://doi.org/10.1109/TMTT.2016.2645154.
[31] H. Sueyoshi, T. Honbo, Effect of copper oxide on microwave heating of copper powder, Powder Metall. 52 (2009) 12–16, https://doi.org/10.1179/174329008X354833.
[32] M.M. Mahmoud, G. Link, M. Thumm, The role of the native oxide shell on the microwave sintering of copper metal powder compacts, J. Alloys Compd. 627 (2015) 231–237, https://doi.org/10.1016/j.jallcom.2014.11.180.
[33] A. Mostovshchikov, F. Gubarev, O. Nazarenko, A. Pestryakov, Influence of short-pulse microwave radiation on thermochemical properties aluminum micropowder, Materials 16 (2023) 951, https://doi.org/10.3390/ma16030951.
[34] H. Nirschl, X. Guo, Characterisation of structured and functionalised particles by small-angle X-ray scattering (SAXS), Chem. Eng. Res. Des. 136 (2018) 431–446, https://doi.org/10.1016/j.cherd.2018.06.012.
[35] W. Zheng, Y. Chen, X. Peng, K. Zhong, Y. Lin, Z. Huang, The phase evolution and physical properties of binary copper oxide thin films prepared by reactive magnetron sputtering, Materials 11 (2018) 1253, https://doi.org/10.3390/ma11071253.
[36] Y. Li, M. Sun, S. Ren, H. Ling, T. Hang, A. Hu, M. Li, The influence of non-uniform copper oxide layer on tin whisker growth and tin whisker growth behavior in SnAg microbumps with small diameter, Mater. Lett. 258 (2020) 126773, https://doi.org/10.1016/j.matlet.2019.126773.
[37] M. Musztyfaga-Staszuk, D. Janicki, K. Gawlińska-Nęcek, R. Socha, G. Putynkowski, P. Panek, Copper oxides on a Cu sheet substrate made by laser technique, Materials 13 (2020) 3794, https://doi.org/10.3390/ma13173794.
[38] M.M. Mahmoud, Characterization of the native oxide shell of copper metal powder spherical particles, Materials 15 (2022) 7236, https://doi.org/10.3390/ma15207236.
[39] D.J. Bergman, D. Stroud, Physical properties of macroscopically inhomogeneous media, in: H. Ehrenreich, D. Turnbull (Eds.), Solid State Physics: Advances in Research and Applications, vol. 46, Academic Press, New York, 1992, pp. 147–269.
[40] A.H. Sihvola, Electromagnetic Mixing Formulas and Applications, Institution of Electrical Engineers, London, 1999.
[41] D.A.G. Bruggeman, Berechnung Verschiedener Physikalischer Konstanten von Heterogenen Substanzen, I. Dielektriziätskonstanten und Leitfähigkeiten der Mischkörper aus Isotropen Substanzen, Ann. Phys-Berlin, Series 5 (24) (1935) 636–679, https://doi.org/10.1002/andp.19354160705.
[42] K.I. Rybakov, I.I. Volkovskaya, Electromagnetic field effects in the microwave sintering of electrically conductive powders, Ceram. Int. 45 (2019) 9567–9572, https://doi.org/10.1016/j.ceramint.2018.10.037.
[43] I.I. Volkovskaya, V.E. Semenov, K.I. Rybakov, Effective high-frequency permeability of compacted metal powders, Radiophys. Quantum Electron. 60 (2018) 797–807, https://doi.org/10.1007/s11141-018-9848-9.
[44] I.S. Grigor'ev, E.Z. Meilikhov (Eds.), Physical Quantities: Handbook, Energoatomizdat, Moscow, 1991.
[45] S. Suda, S. Fuhitsu, K. Koumoto, H. Yanagida, The effect of atmosphere and doping on electrical conductivity of CuO, Jpn. J. Appl. Phys. 31 (1992) 2488–2491, https://doi.org/10.1143/JJAP.31.2488.
[46] M.A. Malik, Nitric oxide production by high voltage electrical discharges for medical uses: a review, Plasma Chem. Plasma Process. 36 (2016) 737–766, https://doi.org/10.1007/s11090-016-9698-1.
[47] K. Birkeland, On the oxidation of atmospheric nitrogen in electric arcs, Trans. Faraday Soc. 2 (1906) 98–116, https://doi.org/10.1039/TF9060200098.
[48] H.S. Eyde, The manufacture of nitrates from the atmosphere by the electric arc – Birkeland-Eyde process, J. Roy. Soc. Arts 57 (2949) (1909) 568–576. https://www.jstor.org/stable/41338647.
[49] D.J. Bergman, Y. Imry, Critical behavior of the complex dielectric constant near the percolation threshold of a heterogeneous material, Phys. Rev. Lett. 39 (1977) 1222–1225, https://doi.org/10.1103/PhysRevLett.39.1222.
[50] C.-W. Nan, Y. Shen, J. Ma, Physical properties of composites near percolation, Annu. Rev. Mater. Res. 40 (2010) 131–151, https://doi.org/10.1146/annurev-matsci-070909-104529.
[51] A.V. Neimark, Electrophysical properties of a percolation layer of finite thickness, Sov. Phys. JETP 71 (1990) 341–349.
[52] G.V. Samsonov, The Oxide Handbook, Plenum, New York, 1973.